Towards Personalized Autism Diagnosis: Promising Results

Y. ElNakieb, et al.

2018 24th International Conference on Pattern Recognition (ICPR)

NeuroSpectrum Insights, Inc.
info@neurospectruminsights.com
www.neurospectruminsights.com

2018 24th International Conference on Pattern Recognition (ICPR)
Beijing, China, August 20-24, 2018

Towards Personalized Autism Diagnosis: Promising Results

Y. ElNakieb[‡], M. Nitzken[†], A. Shalaby[‡], O. Dekhil[*], A. Mahmoud[†], A. Switala[‡], A. Elmaghraby[*], R. Keynton[‡], M. Ghazal[¶], A. Khalil[‖], G. Barnes[§] and A. El-Baz[‡]
[*] Computer Engineering and Computer Science Department, University of Louisville
[†] Department of Electrical and Computer Engineering, University of Louisville
[‡] Department of Bioengineering, University of Louisville
[§] Department of Neurology, University of Louisville
[¶] Electrical and Computer Engineering Department, Abu Dhabi University
[‖] Computer Science and Information Technology Department, Abu Dhabi University

***Abstract*—The ultimate goal of this paper is to develop a novel personalized comprehensive computer aided diagnostic (CAD) system for precise diagnosis of autism spectrum disorder (ASD) based on the 3D shape analysis of the cerebral cortex (Cx). To achieve the main goal of the proposed system, we used structural MRI modality (sMRI) to be able to extract the shape features of the brain cortex. After segmenting the brain cortex from sMRI, we used a spherical harmonics analysis to measure the surface complexity, in addition to studying surface curvatures. Finally, a multi-stage deep network based on several autoencoders and softmax classifiers is constructed to provide the final global diagnosis. The presented CAD system was tested on several datasets, achieving an average accuracy of 92.15%. In addition to its global diagnostic accuracy, the local diagnostic accuracies of the most significant areas also demonstrated the ability of the proposed system to construct very promising local maps of ASD-related brain abnormalities, which can be considered an important step towards personalized medicine for autistic individuals.**

I. Introduction

Autism spectrum disorder (ASD) is a neurodevelopmental syndrome that directly affects communication and social interaction [1]–[8]. However, the ASD causes are not fully understood, and as a result, numerous hypotheses and theories have been proposed for the etiology underlying the disorder. Some investigators have hypothesized that ASD is linked to structural or connectivity abnormalities [9], whereas others have suggested ASD correlates with brain activation while performing different tasks [10], [11]. In order to study various types of abnormalities correlated with ASD, several imaging modalities have been previously employed, such as: (i) structural MRI (sMRI) for anatomical abnormalities, (ii) functional MRI (fMRI) for brain activation abnormalities, and (iii) diffusion tensor imaging (DTI) for connectivity abnormalities. This paper aims to understand and assess ASD by exploiting the findings from sMRI.

For sMRI analysis of anatomical abnormalities, many studies reported abnormalities in the cortical folding of autistic subjects brains. For example, in [12] cortical folding was measured using the gyrification index (GI), a simple measure of non-convexity derived from a single MRI slice or a series of slices. In [12], [13], the GI was found to be larger in autistic children than in typically developed children. More robust shape indices have been derived from spherical harmonic-based shape models of the cerebral cortex [14] and other brain structures [15]. This approach has recently been generalized (HyperSPHARM) to model multiple, disconnected structures simultaneously [16]. Others have used local estimates of surface curvature directly to measure cortical folding and to detect anatomical variation in ASD [17]. For example, Awate et al. [18] reported increased folding in the frontal, parietal and temporal lobes of individuals with ASD compared to typically developed subjects. A study of the curvature of the white matter surface in an independent sample obtained similar results [9]. Besides curvature, differences in sulcal depth have also been investigated, with deeper sulci in anterior insula and in frontal and parietal opercula detected in ASD patients [19].

Although there have been numerous efforts to assess ASD using imaging, until now there is to date no computer-aided diagnosis (CAD) system that is able to diagnose ASD and locate the affected individual on the spectrum. This is where the idea of integrating different modalities originates in order to develop a comprehensive CAD system that can resolve autism endophenotypes and help the clinician deliver personalized treatments to individuals with ASD.

II. Methodology

The objective of the framework was to extract local features from sMRI modality, then use them to obtain a global decision for the subject. More details and experimental results about the proposed framework will be discussed in the next sections.

A. Cortical Shape Analysis

Following the hypothesis that autistic subjects have higher cortical foldings and different brain texture [12], it becomes important to quantify and analyze the cortex shape and brain surface complexity in both autistic and typically developed subjects. To study the cortex shape, two curvature metrics were used, and to study the brain surface complexity, a recently developed approach based on spherical harmonics [20] was used. Both shape and surface features were first studied locally on the Brodmann areas level [21], then fused to obtain an

978-1-5386-3788-3/18/$31.00 ©2018 IEEE

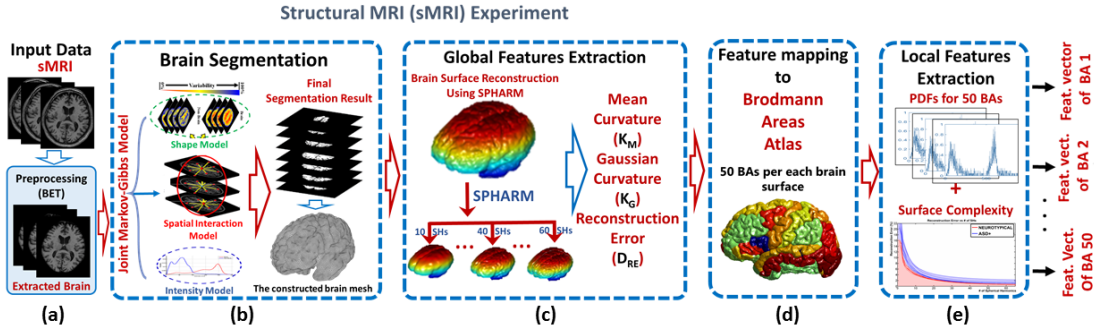

Fig. 1: sMRI experiment pipeline, where brain is extracted, segmented, reconstructed, then features are extracted. For each Brodmann Area (BA), the probability distribution functions of two curvatures metrics and the surface complexity obtained from spherical harmonics reconstruction error using different number of coefficients are calculated.

sMRI based diagnosis decision. To extract the cerebral cortex, there are two important steps applied to the input volumes:

1) *Brain extraction (Skull stripping):* In this study, a modified version of Brain Extraction Tool (BET) explained in [22] was used, where an evolving deformable model was applied to fit the brain surface. BET is a very fast algorithm that needs no preprocessing steps.
2) *Cortex segmentation:* In this study, the segmentation algorithm used was introduced in [20], [23], in which the evolution of a 3D deformable model is constrained using both prior and current appearance models. The prior model used was a 3D Markov-Gibbs random field (MGRF), while the current appearance model is a linear combinations of discrete Gaussian (LCDG) [22], [24].

Cortical complexity analysis using spherical harmonics:

Spectral SPHARM analysis [25] considers a set of 3D surface data as a linear combination of specific basis functions. We perform a weighted-SPHARM analysis similar to the algorithm described in [26]. The surface manifold of the brain cortex is approximated using a triangulated 3D mesh, having 50,000 nodes, constructed using an algorithm based on the work of Fang and Boas [27](Fig. 2). Secondly, the brain cortex mesh for each subject is mapped to a unit sphere utilizing a novel mapping approach [20], called "*Attraction-Repulsion*" that calls for all the mesh nodes to meet two conditions: (*i*) the unit distance of each node from the brain cortex center,

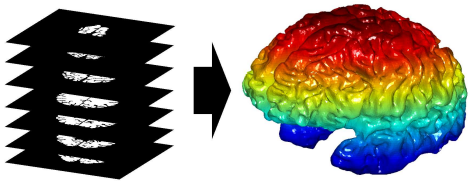

Fig. 2: Illustrating the process of generating a high-resolution 3D mesh for the brain cortex surface from a stack of successive segmented 2D T1-weighted MR image slices.

and (*ii*) an equal distance of each node from all of its nearest neighbors. The brain cortex mesh is then approximated using a linear combination of Spherical Harmonics. In general, the theory is that lower-order harmonics are sufficient to represent the more generic shape information of the cortex. The higher-order harmonics contain the fine details of the brain cortex and help to rebuild the nuanced gyrifications of the brain shape. A SPHARM analysis is performed by solving an isotropic iterative residual fitting for the cortex surface on the unit sphere [25]. Let $\mathcal{S} : \mathbf{M} \rightarrow \mathbf{U}$ denote the mapping of a cortical mesh $\mathbf{M}$ to the unit sphere $\mathbf{U}$. Each node $\mathbf{P} = (x, y, z) \in \mathbf{M}$ mapped to the spherical position $\mathbf{u} = S(\mathbf{P})$ is represented by the spherical coordinates $\mathbf{u} = (\sin\theta\cos\varphi, \sin\theta\sin\varphi, \cos\theta)$ where $\theta \in [0, \pi]$ and $\varphi \in [0, 2\pi)$ are the polar and azimuth angles, respectively. The SH $Y_{\alpha\beta}$ of degree α and order β is defined as [28]:

$$Y_{\alpha\beta} = \begin{cases} c_{\alpha\beta} G_\alpha^{|\beta|} \cos\theta \sin(|\beta|\varphi) & -\alpha \le \beta \le -1 \\ \frac{c_{\alpha\beta}}{\sqrt{2}} G_\alpha^{|\beta|} \cos\theta & \beta = 0 \\ c_{\alpha\beta} G_\alpha^{|\beta|} \cos\theta \cos(|\beta|\varphi) & 1 \le \beta \le \alpha \end{cases} \quad (1)$$

where $c_{\alpha\beta} = \left(\frac{2\alpha+1}{2\pi}\frac{(\alpha-|\beta|)!}{(\alpha+|\beta|)!}\right)^{\frac{1}{2}}$ and $G_\alpha^{|\beta|}$ is the associated Legendre polynomial of degree α and order β. For the fixed α, the polynomials G_α^β are orthogonal over the range $[-1, 1]$. As shown in [28], the Legendre polynomials are an effective means of calculating SHs, and this is the main motivation behind their use in this work.

The brain cortex can be simply reconstructed from the SPHARMs of Eq. (1). In the case of a SPHARM expansion, the standard least-square fitting does suffers from some inaccuracy with the complexity of the 3D shape of the brain cortex, and may inadvertently alter some information that can be used to discriminate between ASD and control individuals. To address this problem, the reconstructed mesh is then smoothed using Laplacian smoothing algorithm described in [29].

To perform a quantitative analysis of the brain shape we propose two techniques for measuring the complexity of the

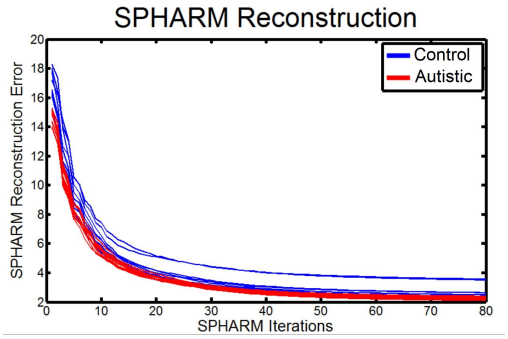

Fig. 3: Estimation of the spherical harmonics surface complexity for the SPHARM reconstruction error. ASD (red) and control (blue) subjects are shown.

cerebral cortex: SPHARM reconstruction error and surface complexity.

SPHARM reconstruction error: Due to the unit sphere mapping, the original brain cortex mesh for each subject is inherently aligned with the mesh that is the SPHARM approximation. As the brain is reconstructed, we can measure the error (using Euclidean distance) between the original brain mesh nodes and the SPHARM approximated brain mesh nodes. This error generates a reconstruction error curve that is unique to each subject as shown in Fig. 3. Unlike our previous work [20] that narrowly examined the first few interactions between individual reconstructions, we propose that examining the area under each of these curves will serve as a more robust metric for the cerebral cortex.

Surface complexity: We also propose a new metric for examining the complexity of the cerebral cortex using the SPHARM coefficients. For a unit sphere f, having a SPHARM expansion as shown in Eq. (1), we compute the surface complexity metric. $S(f)$ is defined as:

$$\begin{aligned} S(f) &= \sum_{L=0}^{\infty} \varepsilon_L^2 \\ &= \sum_{L=0}^{\infty} L B_L^2 \end{aligned} \tag{2}$$

where L is the number of harmonics, and b are the previously

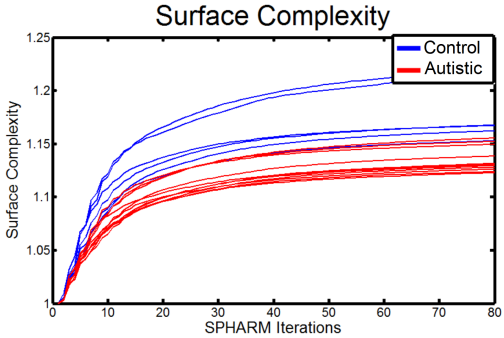

Fig. 4: Estimation of the spherical harmonics surface complexity for the surface complexity. ASD (red) and control (blue) subjects are shown.

calculated SPHARM coefficients. The squared residual ε_L^2 is defined as:

$$\begin{aligned} \varepsilon_L^2 &= \|f - f_L\|^2 \\ &= \|\sum_{l=L+1}^{\infty} \sum_{m=-l}^{l} b_{lm} Y_l^m\|^2 \\ &= \sum_{l=L+1}^{\infty} \sum_{m=-l}^{l} |b_{lm}|^2 \\ &= \sum_{l=L+1}^{\infty} B_l^2 \end{aligned} \tag{3}$$

For use in 3-dimensional SPHARM analysis there are three sets of coefficients for each direction, x, y and z. Therefore the surface complexity is expanded from Equ. 3 to be defined as:

$$S(f) = \frac{\sum_{L=0}^{\infty} L(B_{L,x}^2 + B_{L,y}^2 + B_{L,z}^2)}{\|f_x\|^2 + \|f_y\|^2 + \|f_z\|^2} \tag{4}$$

This metric generates a unique curve for each subject similar to the SPHARM reconstruction error curves, as shown in Fig. 4. Some of the advantages to this calculation are that it relies solely on the coefficients, making it a self contained metric, and it serves to represent the average degree of SPHARM expansion. It is also a convergent metric, and can be computed over the range of harmonics of interest. The surface complexity is a second unique metric for examining the cerebral cortex. Fig. 1 shows the whole process of sMRI experiment.

Curvature analysis: Another metric used for discrimination between autistic and typically developed subjects is the principal curvatures. In this experiment, the two principal curvatures κ_1, κ_2 [30] were calculated at each mesh vertex. Using the calculated principal curvatures, two metrics were calculated [26]: (i) Gaussian curvature, $K_G = \kappa_1 \kappa_2$ and (ii) mean curvature $K_M = \frac{1}{2}(\kappa_1 + \kappa_2)$ (Fig. 1.c).

Brain parcellation into Brodmann areas: After calculating the above two metrics at each vertex, it is important to allocate those metric values into local brain regions. In this experiment, the parcellation of the cerebral cortex into Brodmann areas (BAs) [21] was used. BAs are regions of cerebral cortex defined based on cell histological structures. Although there are 43 BAs defined per hemisphere, only 25 BAs per hemisphere were used in this experiment. This is due to the fact that the analysis done in this experiment is a surface analysis, not a volumetric one, and not all BAs appear on the brain surface [26]. For each of the used BAs both cortical complexity and curvature metrics are calculated to be used in the local classification level (Fig. 1.d and e).

B. Local and Global ASD Diagnosis

Using the local features extracted from sMRI, both local and global analysis were provided. On the local level, each of the Brodmann areas were used separately to distinguish between autistic and typically developed subjects. Since distinct areas contain different numbers of voxels or vertices, a more convenient way than using raw data to represent features is to use the data probability distribution functions (PDFs) of features with a fixed number of samples at each area (typically 500 sample per PDF were used in this experiment). For reconstruction error and surface complexity, the raw data was used because it is defined on the area level, not on vertex level. After preparing features and presenting them in

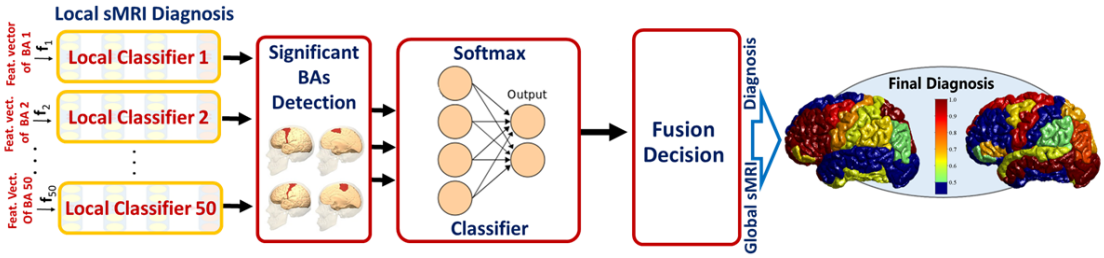

Fig. 5: After extracting local features form sMRI, they are fed to local classification stage to extract the significant areas per this modality. Those areas are then fused to obtain a subject global decision.

a convenient way, higher level features were extracted using an autoencoder trained for each area. A stacked non-negativity constraint autoencoder (SNCAE) [31] was used for this task. The intuition behind using the SNCAE is to map higher dimensional data to a lower dimensional space while keeping the most characteristic features of the original input data. This is obtained by minimizing the reconstruction error between the initial input data and the reconstructed data from the lower dimensional space. The cost function of the SNCAE is defined as:

$$J_{SAE}(w,b) = J_E(W,b) + \beta J_{kl}(\rho||\hat{\rho}) + \frac{\lambda}{2}\sum_{l=1}^{2}\sum_{i=1}^{s_l}\sum_{j=1}^{s_j+1}(\omega_{ij}^{l})^2 \quad (5)$$

where w is the set of weight that maps input to lower dimensional space, b is the layer nodes biases, J_E is the reconstruction error, β controls the sparsity penalty, $J_{kl}(\rho||\hat{\rho})$ is the sparsity term, ρ is the desired activation proportion, $\hat{\rho}$ is the vector of average hidden activities, λ controls the penalty term facilitating weight decay to prevent overfitting, s_l and s_{l+1} are the sizes of adjacent layers.

The weights are randomly initialized then updated using batch gradient descent, where L-BFGS optimization algorithm is used [32].

Local diagnosis decisions were then obtained using a softmax classifier that takes higher level features as inputs and outputs a probability that a specific area belongs to an autistic subject. Normally, not all areas will give significant discrimination between autistic and typically developed subjects; thus, to obtain a global decision for a subject, only the significant areas were used.

For each subject, the higher level features extracted from significant areas were fused, fed to an autoencoder, then classified using a softmax classifier that outputs the probability that a subject is autistic. Fig. 5 shows the entire diagnosis pipeline.

III. Experimental Results

Data for this experiment were obtained from several multicenter databases. Data for validation comes from authoritative resources including the National Database of Autism Research (NDAR), The Autism Brain Imaging Data Exchange (ABIDE), and Infant Brain Imaging Symposium (IBIS). Three ABIDE databases were tested. The global ABIDE database is divided by each of the participating centers. Each centers database contains a roughly even distribution of neurotypical and ASD individuals. The databases selected for analysis were the Kennedy Krieger Institute (KKI), University of California, Los Angeles (UCLA), and the University of Michigan (UM). These databases were selected from within the global database, because these sets offered the largest unique pools of individual brain scans available for testing. A total of 238 individual subjects were analyzed and classified from the ABIDE data exchange. Additional data from sources including the NDAR Tom Conturo/University of Pittsburgh database and the IBIS database were also tested. These databases contain 46 and 36 subjects, respectively.

A. Kennedy Krieger Institute Results

The ABIDE Kennedy Krieger Institute (KKI) database was collected from individuals between the ages of 7 to 12 years of age, with an average age of 10 years. Subjects were evaluated using the WISC, ADOS, and by medical professionals to determine a diagnosis. All scans were acquired using the MP-RAGE, three-dimensional, T1-weighted, gradient-echo sequence. The results for the KKI database showed an overall accuracy of 88.89%. Assuming negative for diagnosing autism and positive for determining neurotypical, the test sensitivity (TPR) is 0.939, the specificity (SPC) is 0.810, the positive predictive value (PPV) is 0.886, and the negative predictive value (NPV) is 0.895.

B. University of California, Los Angeles Results

The University of California, Los Angeles (UCLA) database was collected from individuals between the ages of 8 to 17 years of age, with an average age of 13 years. Subjects were evaluated using the WISC, ADOS, and by medical professionals to determine a diagnosis. All scans were acquired using the MP-RAGE, three-dimensional, T1-weighted, gradient-echo sequence. The results for the UCLA database showed an overall accuracy of 94.36%. Assuming negative for

diagnosing autism and positive for determining neurotypical, TPR is 0.900, SPC is 0.976, PPV is 0.964, and NPV is 0.930.

C. University of Michigan Results

The University of Michigan (UM) database was collected from individuals between the ages of 8 to 18 years of age, with an average age of 13 years. Subjects were evaluated using the WISC, ADOS,and by medical professionals to determine a diagnosis. All scans were acquired using the MP-RAGE, three-dimensional, T1-weighted, gradient-echo sequence. The results for the UM database showed an overall accuracy of 88.18%. Assuming negative for diagnosing autism and positive for determining neurotypical, TPR is 0.872, SPC is 0.890, PPV is 0.889, and NPV is 0.875.

D. NDAR Conturo Results

The NDAR Conturo database contains information from 46 subjects. The Conturo database was collected from individuals between the ages of 10 to 30 years of age, with an average age of 21 years. Subjects were evaluated using the ADI-R, ADOS, and by medical professionals to determine a diagnosis. All scans were acquired using a standard T1-weighted saggital plane acquisition. Images were rotated to the axial plane for processing. The results for the Conturo database showed an overall accuracy of 95.65%. Assuming negative for diagnosing autism and positive for determining neurotypical, TPR is 1.000, SPC is 0.920, PPV is 0.913, and NPV is 1.000.

E. Infant Brain Imaging Study Results

A subset of the complete IBIS database was provided for evaluation purposes consisting of 36 subjects. The Infant Brain Imaging Study (IBIS) database was collected from individuals between the ages of 6 to 9 months of age, with an average age of 7.5 months. Subjects were diagnosed as they grew older using the ADI-R, ADOS, and by medical professionals to determine a diagnosis. MRI brain scans were completed at the clinical sites on identical 3-T Siemens TIM Trio scanners (Siemens Medical Solutions, Malvern, Pa.) equipped with 12-channel head coils during natural sleep. The diffusion tensor imaging sequence was acquired as an ep2d_diff pulse sequence with a field of view of 190 mm, 7581 transversal slices, a slice thickness of 2mm isotropic, 2*2*2-mm3 voxel resolution, a TE of 102 ms, variable b values between 0 and 1,000s/mm2, 25 gradient directions, and a scan time of 56 minutes.The results for the IBIS database showed an overall accuracy of 97.29%. Assuming negative for diagnosing autism and positive for determining neurotypical, TPR is 0.964, SPC is 1.000, PPV is 1.000, and NPV is 0.889.

F. Personalized diagnosis

We here emphasize the system capability to identify the localized abnormalities for each individual subject. In addition to reporting the global diagnostic result, a detailed report is generated to show a personalized local diagnosis for every subject. Using this report, a color-coded brain map is generated to show the most affected areas with autism-related impairments.

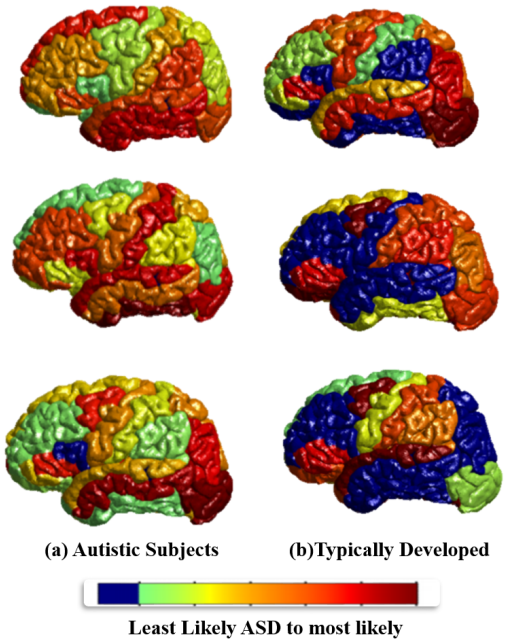

Fig. 6: sMRI personalized brain cortex local results of 6 subjects. The (a) are autistic subjects, and (b) are typically developed. As shown, autistic subjects have more impacted areas than the healthy typically developed ones. The meshes are color coded to indicate the strength of association of each BA with the ASD. Blue is the least belonging to autistic class, and red is the most belonging to it.

Fig.6 shows 4 samples of the color-coded brain maps of the brain cortex obtained from sMRI, with the associated color code used.

IV. Conclusion and Future Work

This framework is very promising as it achieves several goals. First, it provides very high local accuracies, so that in addition to deciding whether a subject is autistic, it allow for a better understanding of the areas of the cerebral cortex impacted by ASD, which in turn should lead to more predictability and understanding of autistic individuals' behavior. Second, our system demonstrated scalability, where additional imaging modalities or data sources could be integrated to the model, and its contribution could be considered separately or jointly with other data sources.

Yet there are many challenges and enhancements to be considered in future work. Although the system is well tested and its robustness is assured, more data is needed to check the extendibility and generalization of the results. Also, more medical interpretation and statistical analysis are needed to map the impacted regions to the corresponding expected

behaviors. The next steps for this CAD system are to include more data and plugging other modalities (functional MRI and/or DTI). In this way, the CAD system will be able to study shape, connectivity and functionality, which might be a big step towards an integrated full system for autism prediction, diagnosis and personalization.

V. Acknowledgment

Data and/or research tools used in the preparation of this manuscript were obtained from the NIH- supported National Database for Autism Research (NDAR). NDAR is a collaborative informatics system created by the National Institutes of Health to provide a national resource to support and accelerate research in autism. Dataset identifier(s): 6, 19. This manuscript reflects the views of the authors and may not reflect the opinions or views of the NIH or of the Submitters submitting original data to NDAR.

ABIDE/KKI was funded by the NINDS (R01 NS048527) and the Autism Speaks Foundation. ABIDE/UCLA was funded by the UCLA Autism Center of Excellence, NICHD (P50 HD055784), and NIMH (R01 HD065280). ABIDE/UM was funded by Autism Speaks, Mighigan Institue for Clinical and Health Research, and NIH (U19 HD035482, MH066496, and R21 MH079871).

References

[1] American Psychiatric Association, *Diagnostic and statistical manual of mental disorders, fifth edition (DSM-5)*. Arlington: American Psychiatric Association, 2013.

[2] M. F. Casanova, A. El-Baz, and J. S. Suri, *Autism Imaging and Devices*. CRC Press, 2017.

[3] M. F. Casanova, A. S. El-Baz, J. S. Suri *et al.*, *Imaging the brain in autism*. Springer, 2013.

[4] E. M. Sokhadze, A. Tasman, G. E. Sokhadze, A. S. El-Baz, and M. F. Casanova, "Behavioral, cognitive, and motor preparation deficits in a visual cued spatial attention task in autism spectrum disorder," *Applied psychophysiology and biofeedback*, vol. 41, no. 1, pp. 81–92, 2016.

[5] M. Ismail, R. Keynton, M. Mostapha, A. ElTanboly, M. Casanova, G. Gimel'farb, and A. El-Baz, "Studying autism spectrum disorder with structural and diffusion magnetic resonance imaging: a survey," *Frontiers in human neuroscience*, vol. 10, 2016.

[6] Y. Wang, E. M. Sokhadze, A. S. El-Baz, X. Li, L. Sears, M. F. Casanova, and A. Tasman, "Relative power of specific eeg bands and their ratios during neurofeedback training in children with autism spectrum disorder," *Frontiers in human neuroscience*, vol. 9, 2016.

[7] E. M. Sokhadze, J. Frederick, Y. Wang, M. Kong, A. S. El-Baz, A. Tasman, and M. F. Casanova, "Event-related potential (erp) study of facial expression processing deficits in autism." *Journal of Communications Research*, vol. 7, no. 4, 2015.

[8] A. Elnakib, M. F. Casanova, G. Gimelfarb, and A. El-Baz, "Autism diagnostics by 3d shape analysis of the corpus callosum," in *Machine Learning in Computer-aided Diagnosis: Medical Imaging Intelligence and Analysis*. IGI Global, 2012, pp. 315–335.

[9] M. Ismail *et al.*, "Detection of white matter abnormalities in MR brain images for diagnosis of autism in children," in *Biomedical Imaging (ISBI), 2016 IEEE 13th International Symposium on*. IEEE, 2016.

[10] N. Barnea-Goraly *et al.*, "White matter structure in autism: preliminary evidence from diffusion tensor imaging," *Biological Psychiatry*, vol. 55, no. 3, pp. 323–326, 2004.

[11] O. Dekhil, M. Ismail, A. Shalaby, A. Switala, A. Elmaghraby, R. Keynton, G. Gimel'farb, G. Barnes, and A. El-Baz, "A novel cad system for autism diagnosis using structural and functional mri," in *Biomedical Imaging (ISBI 2017), 2017 IEEE 14th International Symposium on*. IEEE, 2017, pp. 995–998.

[12] A. Y. Hardan *et al.*, "Increased frontal cortical folding in autism: a preliminary MRI study," *Psychiatry Research: Neuroimaging*, vol. 131, no. 3, pp. 263–268, 2004.

[13] A. El-Baz, M. F. Casanova, G. Gimelfarb, M. Mott, and A. E. Switala, "Autism diagnostics by 3d texture analysis of cerebral white matter gyrifications," in *International Conference on Medical Image Computing and Computer-Assisted Intervention*. Springer, 2007, pp. 882–890.

[14] E. L. Williams *et al.*, "Spherical harmonic analysis of cortical complexity in autism and dyslexia," *Translational Neuroscience*, vol. 3, no. 1, pp. 36–40, 2012.

[15] C. Scanlon *et al.*, "Cortical thinning and caudate abnormalities in first episode psychosis and their association with clinical outcome," *Schizophrenia Research*, vol. 159, no. 1, pp. 36–42, 2014.

[16] A. P. Hosseinbor *et al.*, "4D hyperspherical harmonic (HyperSPHARM) representation of surface anatomy: a holistic treatment of multiple disconnected anatomical structures," *Medical Image Analysis*, vol. 22, no. 1, pp. 89–101, 2015.

[17] M. F. Casanova, A. El-Baz, A. Elnakib, A. E. Switala, E. L. Williams, D. L. Williams, N. J. Minshew, and T. E. Conturo, "Quantitative analysis of the shape of the corpus callosum in patients with autism and comparison individuals," *Autism*, vol. 15, no. 2, pp. 223–238, 2011.

[18] S. P. Awate *et al.*, "3D cerebral cortical morphometry in autism: Increased folding in children and adolescents in frontal, parietal, and temporal lobes," in *International Conference on Medical Image Computing and Computer-Assisted Intervention*. Springer, 2008.

[19] C. W. Nordahl *et al.*, "Cortical folding abnormalities in autism revealed by surface-based morphometry," *The Journal of Neuroscience*, vol. 27, no. 43, pp. 11 725–11 735, 2007.

[20] M. Nitzken *et al.*, "3d shape analysis of the brain cortex with application to dyslexia," in *Image Processing (ICIP), 2011 18th IEEE International Conference on*. IEEE, 2011, pp. 2657–2660.

[21] L. J. Garey, Ed., *Brodmann's 'localisation in the cerebral cortex'*. London: World Scientific, 1994.

[22] A. Alansary *et al.*, "Infant brain extraction in T1-weighted MR images using BET and refinement using LCDG and MGRF models," *IEEE Journal of Biomedical and Health Informatics*, vol. 20, no. 3, pp. 925–935, 2016.

[23] A. El-Baz *et al.*, "Stochastic modeling for medical image analysis,," *Taylor and Francis*, January 2016.

[24] A. A. Farag *et al.*, "Precise segmentation of multimodal images," *IEEE Transactions on Image Processing*, vol. 15, April 2006.

[25] M. K. Chung, K. M. Dalton, L. Shen, A. C. Evans, and R. J. Davidson, "Weighted fourier series representation and its application to quantifying the amount of gray matter," *Medical Imaging, IEEE Transactions on*, vol. 26, no. 4, pp. 566–581, 2007.

[26] M. J. Nitzken, "Shape analysis of the human brain," Ph.D. dissertation, University of Louisville, 2015.

[27] Q. Fang and D. A. Boas, "Tetrahedral mesh generation from volumetric binary and grayscale images," in *Biomedical Imaging: From Nano to Macro, 2009. ISBI'09. IEEE International Symposium on*. IEEE, 2009, pp. 1142–1145.

[28] R. Courant and D. Hilbert, *Methods of Mathematical Physics*. London: Interscience, 1953, vol. 1.

[29] M. Desbrun *et al.*, "Implicit fairing of irregular meshes using diffusion and curvature flow," in *Proceedings of the 26th annual conference on Computer graphics and interactive techniques*. ACM Press/Addison-Wesley Publishing Co., 1999, pp. 317–324.

[30] B. Hamann, "Curvature approximation for triangulated surfaces," in *Geometric modelling*, G. Farin *et al.*, Eds. New York: Springer, 1993, pp. 139–153.

[31] E. Hosseini-Asl *et al.*, "Deep learning of part-based representation of data using sparse autoencoders with nonnegativity constraints," *IEEE transactions on neural networks and learning systems*, vol. 27, no. 12, pp. 2486–2498, 2016.

[32] C. Zhu, R. H. Byrd, P. Lu, and J. Nocedal, "Algorithm 778: L-bfgs-b: Fortran subroutines for large-scale bound-constrained optimization," *ACM Transactions on Mathematical Software (TOMS)*, vol. 23, no. 4, pp. 550–560, 1997.